Available online at www.sciencedirect.com
SCIENCE DIRECT®
ELSEVIER
International Journal of Solids and Structures 43 (2006) 475–496
INTERNATIONAL JOURNAL OF SOLIDS and STRUCTURES
www.elsevier.com/locate/ijsolstr

Macroscopic modelling of structured materials: Relationship between orthotropic Cosserat continuum and rigid elements

Siro Casolo *

Dipartimento di Ingegneria Strutturale, Politecnico di Milano, Piazza Leonardo da Vinci, 32, 20133 Milano, Italy

Received 15 September 2004; received in revised form 11 March 2005
Available online 21 April 2005

Abstract

The macroscopic modelling of in-plane elastic behaviour of composite solids made with regular orthotropic texture is the object of the present study. At the macro-scale, the effect of heterogeneity can be included by adopting an homogenisation toward a generalised continuum on which specific finite element codes are based. As an alternative, a specific rigid element approach has been recently proposed [Casolo, S., 2004. Modelling in-plane micro-structure of masonry walls by rigid elements. International Journal of Solids and Structures 41(13), 3625–3641] based on a discrete mechanistic formulation. This paper presents a sequel of such research, and expounds the theoretical relationship between the orthotropic Cosserat continuum and the proposed rigid elements. Then, referring to two different masonry-like textures, the constitutive parameters of the corresponding Cosserat continuum and of the rigid element model are calculated. Numerical analyses compare their performance, and display the impact of the composite texture in the case of a concentrated load. The capability to discern the behaviour of different structured materials at the macro-scale is pointed out by observing how the local rotation of the blocks and the consequent different deformation of vertical and horizontal joints have influence on the strain field maps.

Keywords: Micro–macro; Rigid elements; Cosserat continuum; Homogenisation; Plane elasticity; Masonry texture

* Tel.: +39 2 2399 4356; fax: +39 2 2399 4220.
E-mail address: Siro.Casolo@polimi.it

0020-7683/$ - see front matter © 2005 Elsevier Ltd. All rights reserved.
doi:10.1016/j.ijsolstr.2005.03.037

1. Introduction

The engineering demand for computational models capable to describe the macroscopic mechanical behaviour of complex structures made of heterogeneous solid materials is at the basis of the present research. The impact of heterogeneity at the macro-scale essentially depends on the geometry of internal texture, the difference of mechanical properties of the material components, and the ratio of micro-structure lengths respect to the global size of the system. In particular, micro-structure effects become relevant in the presence of high strain gradient, with softening materials, and complex shear response. Macroscopic models capable to account for the peculiar behaviour of structured materials are particularly required in the field of structural dynamics where engineering applications need the description of the global response of large structures with a reasonable number of degrees of freedom.

In the frame of continuum solid mechanics, homogenisation toward a generalised continuum is often used as the basis for implementation of specific finite element models (e.g. Nakamura et al., 1984; Ristinmaa and Vecchi, 1996; Shu et al., 1999; Providas and Kattis, 2002). The effective determination of the macroscopic constitutive coefficients of a generalised continuum material is clearly the focus of the micro–macro transition procedure. Both analytical and computational approaches have been proposed in literature with reference to the behaviour of periodic heterogeneous materials (Forest and Sab, 1998; van der Sluis et al., 1999; Bouyge et al., 2001; Forest et al., 2001). In particular, the case of two-dimensional periodic rigid block assemblies has been modelled by adopting an orthotropic Cosserat continuum (Mühlhaus, 1993; Masiani et al., 1995; Sulem and Mühlhaus, 1997; Trovalusci and Masiani, 1999).

A specific rigid element model has been recently proposed as an alternative computational method (Casolo, 2004). Following an engineering approach, the heterogeneous solid material is imaged as a "mechanism" made by the assembly of rigid elements connected by simple elastic springs, in the spirit of the rigid body spring model, RBSM (Kawai, 1978; Griffiths and Mustoe, 2001). These elastic devices are defined by a direct discrete formulation that does not need a differential formulation of the field equations for the solid material (Tonti, 2001). Focusing on the global dynamic response, at a level of detail that was larger than the size of the minimum periodic cell, the proposed approach proved successful in transferring a memory of the original texture geometry from the composite micro-scale to the elements meso-scale also when adopting very few degrees of freedom.

The sequel of such research is presented in this paper, where the relationship between the proposed mechanistic formulation and the orthotropic Cosserat continuum is expounded with emphasis on the capability of discerning the impact of micro-structure texture at the macro-scale. Numerical applications investigate two orthotropic masonry-like arrangements in the case of a load applied on a small area by adopting different ratios for the elastic moduli of the material components. In these cases the local shear deformation clearly depends on the blocks shape and their geometric arrangement in the composite solid, and the "local" mean rotation of the blocks appears as an important feature that should be accounted in order to include a memory of the micro-structure at a larger scale. These local effects become particularly relevant in the case of large differences in the elastic moduli of the components, as it happens in real masonry walls when mortar joints suffer high mechanical degradation (Trovalusci and Masiani, 2003).

2. Plane orthotropic Cosserat elastic continuum

2.1. Governing equations

The governing equations for the case of a plane solid body $\Omega \subset \Re^2$ made of linear elastic Cosserat material are presented from an engineering point of view. Making reference to the symbols shown in Fig. 1, two

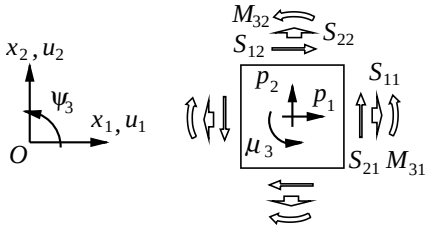

Fig. 1. Adopted notation for the plane Cosserat continuum.

displacements $\{u_1, u_2\}$ and a local rotation ψ_3 are associated to each point, while $S_{\alpha\beta}$ and $M_{3\alpha}$ are the components of the stress and couple stress tensor, respectively.

The field equations and the boundary conditions are:

$$\begin{cases} S_{\alpha\beta,\beta} + p_\alpha = 0 \\ M_{3\alpha,\alpha} + \epsilon_{3\alpha\beta} S_{\beta\alpha} + \mu_3 = 0 \end{cases} \text{in } \Omega$$
$$\begin{cases} S_{\alpha\beta} n_\beta - s_\alpha = 0 \\ M_{3\alpha} n_\alpha - m_3 = 0 \end{cases} \text{on } \partial\Omega \tag{1}$$

where ϵ_{ijk} is the alternating symbol; p_α and μ_3 are respectively the body forces and the body couple; n_1, n_2 are the components of the outward unit normal to the boundary $\partial\Omega$; s_α and m_3 are the prescribed tractions and couples; $\alpha, \beta = 1, 2$. Summation of repeated indexes is implicit. The external virtual work $\mathscr{W}_e$ and the internal virtual work $\mathscr{W}_i$ are defined as follows:

$$\mathscr{W}_e = \int_\Omega (p_\alpha u_\alpha + \mu_3 \psi_3)\, \mathrm{d}V + \int_{\partial\Omega} (s_\alpha u_\alpha + m_3 \psi_3)\, \mathrm{d}A \tag{2}$$

$$\mathscr{W}_i = \int_\Omega \left(S_{\alpha\beta} E_{\alpha\beta} + M_{3\alpha} K_{3\alpha}\right) \mathrm{d}V \tag{3}$$

Balance of work $\mathscr{W}_e = \mathscr{W}_i$ together with the equilibrium equations (1) leads to the definition of strain tensors $E_{\alpha\beta}$ and $K_{3\alpha}$, conjugated in virtual work to the stress and the couple stress tensors, as a function of the displacements and the local rotation

$$\begin{aligned} E_{\alpha\beta} &= u_{\alpha,\beta} + \epsilon_{3\alpha\beta}\psi_3 \\ K_{3\alpha} &= \psi_{3,\alpha} \end{aligned} \tag{4}$$

Eq. (4) shows that shear strains are not symmetric as they are affected by the local rotation ψ_3. In particular, for $\alpha \neq \beta$ it is worth to distinguish a "symmetric shear strain" E_s, a "macro-rotation" E_w, and a "relative micro-rotation" E_ψ as follows (Fig. 2)

$$\left.\begin{aligned} E_s &= \tfrac{1}{2}(u_{1,2} + u_{2,1}) \\ E_w &= \tfrac{1}{2}(-u_{1,2} + u_{2,1}) \\ E_\psi &= E_w - \psi_3 \end{aligned}\right\} \rightarrow \begin{cases} E_{12} = E_s - E_\psi \\ E_{21} = E_s + E_\psi \end{cases} \tag{5}$$

The constitutive relations for a centro-symmetric Cosserat continuum that corresponds to a two-dimensional periodical masonry-like block texture (Trovalusci and Masiani, 1999) can be written as

$$\begin{aligned} S_{\alpha\beta} &= \mathsf{C}_{\alpha\beta\gamma\delta} E_{\gamma\delta} \\ M_{3\alpha} &= \mathsf{D}_{3\alpha3\beta} K_{3\beta} \end{aligned} \tag{6}$$

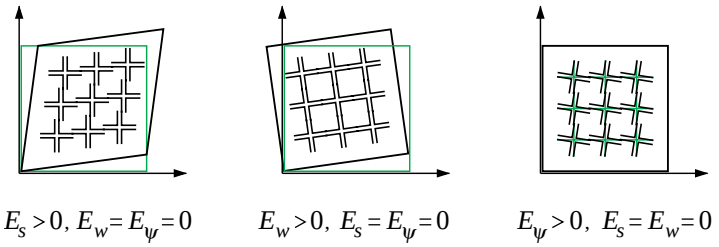

Fig. 2. Simple deformation schemes of plane Cosserat continuum.

or in terms of elastic compliance

$$\begin{aligned} E_{\alpha\beta} &= \mathsf{A}_{\alpha\beta\gamma\delta} S_{\gamma\delta} \\ K_{3\alpha} &= \mathsf{B}_{3\alpha 3\beta} M_{3\beta} \end{aligned} \tag{7}$$

being $\mathsf{A} = \mathsf{C}^{-1}$ and $\mathsf{B} = \mathsf{D}^{-1}$.

In the case of orthotropic texture (Fig. 3) the shear response and the axial response are decoupled, and it is useful to express the elastic tensor of the corresponding hyperelastic Cosserat continuum in a reference frame aligned with the principal axes of the material as follows

$$\begin{Bmatrix} S_{11} \\ S_{22} \\ S_{12} \\ S_{21} \\ M_{31} \\ M_{32} \end{Bmatrix} = \begin{bmatrix} \mathsf{C}_{1111} & \mathsf{C}_{1122} & 0 & 0 & 0 & 0 \\ \mathsf{C}_{1122} & \mathsf{C}_{2222} & 0 & 0 & 0 & 0 \\ 0 & 0 & \mathsf{C}_{1212} & \mathsf{C}_{1221} & 0 & 0 \\ 0 & 0 & \mathsf{C}_{1221} & \mathsf{C}_{2121} & 0 & 0 \\ 0 & 0 & 0 & 0 & \mathsf{D}_{3131} & 0 \\ 0 & 0 & 0 & 0 & 0 & \mathsf{D}_{3232} \end{bmatrix} \begin{Bmatrix} E_{11} \\ E_{22} \\ E_{12} \\ E_{21} \\ K_{31} \\ K_{32} \end{Bmatrix} \tag{8}$$

The shear moduli C_{1212}, C_{1221}, C_{2121} and flexural moduli $\mathsf{D}_{3\alpha 3\alpha}$ specifically characterise the orthotropic Cosserat continuum. In the special case of $\mathsf{C}_{1212} = \mathsf{C}_{1221} = \mathsf{C}_{2121} = G$ the local rotation ψ_3 does not affect the shear stresses that remain always symmetric $S_{12} = S_{21}$.

2.2. Identification of elastic moduli

The elastic parameters of the orthotropic Cosserat continuum have been identified from the two masonry-like composite textures shown in Fig. 3a and b. The dimensions of the rectangular blocks are $2l \times 2h = 25 \times 5.5\ \text{cm}^2$, whereas the side of the square blocks is $2l = 12$ cm. The thickness of all the mortar joints is $t = 1$ cm. An homogeneous isotropic material has been assumed for all the components with a fixed

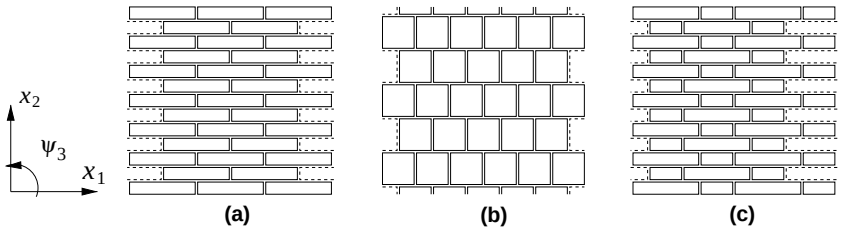

Fig. 3. Examples of orthotropic masonry-like textures.

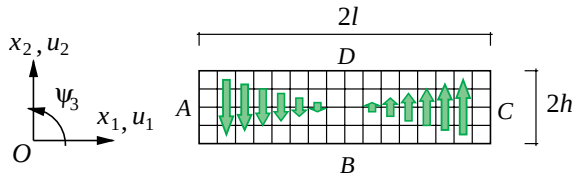

Fig. 4. Finite element mesh of a rectangular block with indication of the points used for measuring the local rotation and the body forces applied as a local couple.

Poisson coefficient $\nu = 0.1$. The elastic modulus of the blocks is $E_b = 10\,000$ MPa, while different values are given to the elastic moduli of the horizontal (E_h) and the vertical (E_v) mortal joints. Since the vertical joints are usually weaker than the horizontal, then a fixed ratio $E_h/E_v = 10$ has been assumed in all the numerical analyses.

A computational approach has been adopted to identify the elastic tensor. The evaluation of axial moduli $C_{\alpha\alpha\beta\beta}$ is straightforward by applying anti-symmetric tractions under symmetric essential boundary conditions (Anthoine, 1995). The evaluation of the shear moduli C_{1212}, C_{1221} and C_{2121} requires some more attention since in the present case all the material components are deformable, i.e. the blocks are not "rigid". As a consequence, it is necessary to define a clear criterion for measuring the mean local rotation of the blocks, and moreover for applying the external loads to the blocks as to reproduce a periodic field of "local" body couples. This is important in order to obtain a good estimate of the mean elastic behaviour also when the ratio of elastic moduli of the blocks and the joints is not very high. According to the scheme shown in Fig. 4, a local couple is obtained as a linear distribution of body forces, while the local rotation angle ψ_3 is given by

$$\psi_3 = \frac{u_2^C - u_2^A}{4l} + \frac{u_1^D - u_1^B}{4h} \tag{9}$$

The three Cosserat shear moduli are obtained by means of the two tests shown in Fig. 5, for which the macro-rotation is null, $E_w = 0$. The test shown on the left side ("symm") is made considering a refined finite element mesh of the representative volume element with periodic displacement boundary conditions and loaded by anti-periodic shear stresses S_s that have equal absolute value on all the four sides. The macroscopic values of E_s and ψ_s are measured on the deformed finite element mesh (Figs. 6 and 7). The test shown on the right side ("skew") considers a representative volume element with displacement boundary conditions that produce null symmetric shear strain, $E_s = 0$, while the periodic local couples μ_3 are applied to the blocks. In this case the macroscopic quantity measured on the finite element meshes (Figs. 6 and 7) is the local rotation ψ_w, and periodicity guarantees that $\mu_3 = S_{12} - S_{21}$ as a consequence of the second row of Eq. (1). The constitutive relations for these two tests are

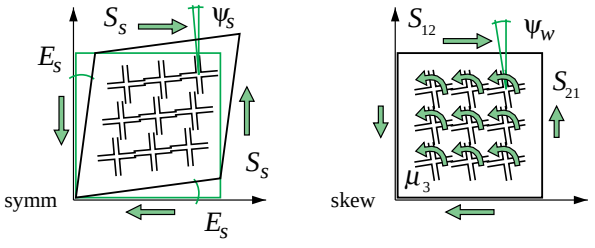

Fig. 5. Scheme of the tests for identification of Cosserat shear elasticities.

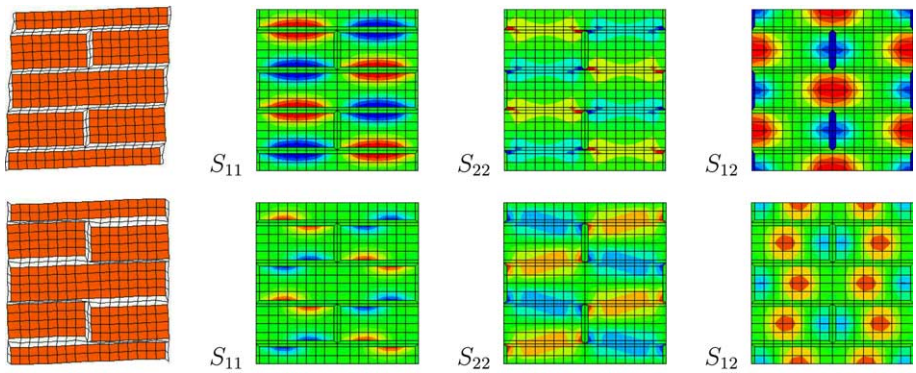

Fig. 6. Deformation and stress maps for a rectangular block texture with $\mathrm{Log}\frac{E_\mathrm{b}}{E_\mathrm{h}} = 2$ and $E_\mathrm{h}/E_\mathrm{v} = 10$. Symmetric shear test ("symm"), in the first row; local couples test ("skew") in the second row.

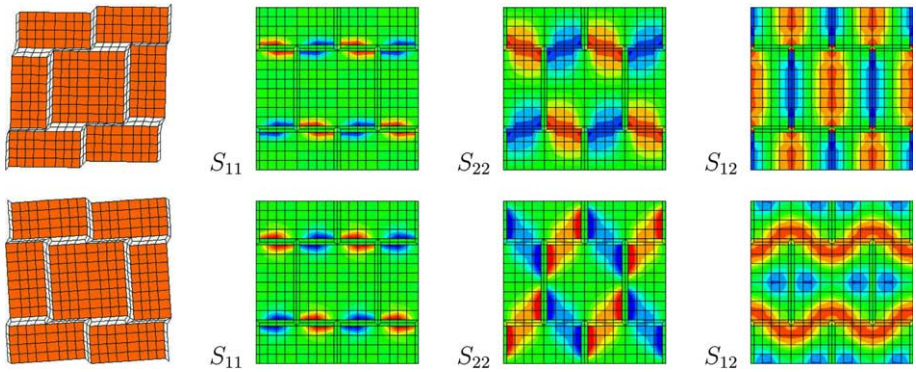

Fig. 7. Deformation and stress maps for a square block texture with $\mathrm{Log}\frac{E_\mathrm{b}}{E_\mathrm{h}} = 2$ and $E_\mathrm{h}/E_\mathrm{v} = 10$. Symmetric shear test ("symm"), in the first row; local couples test ("skew") in the second row.

$$\begin{bmatrix} \mathsf{C}_{1212} & \mathsf{C}_{1221} \\ \mathsf{C}_{1221} & \mathsf{C}_{2121} \end{bmatrix} \begin{Bmatrix} E_\mathrm{s} + \psi_\mathrm{s} \\ E_\mathrm{s} - \psi_\mathrm{s} \end{Bmatrix} = \begin{Bmatrix} S_\mathrm{s} \\ S_\mathrm{s} \end{Bmatrix}$$
$$\begin{bmatrix} \mathsf{C}_{1212} & \mathsf{C}_{1221} \\ \mathsf{C}_{1221} & \mathsf{C}_{2121} \end{bmatrix} \begin{Bmatrix} \psi_\mathrm{w} \\ -\psi_\mathrm{w} \end{Bmatrix} = \begin{Bmatrix} S_{12} \\ S_{21} \end{Bmatrix} \tag{10}$$

By merging these equations, the unknown shear moduli C_{1212}, C_{1221} and C_{2121} are obtained as a solution of the following linear system

$$\begin{bmatrix} E_\mathrm{s} + \psi_\mathrm{s} & E_\mathrm{s} - \psi_\mathrm{s} & 0 \\ 0 & E_\mathrm{s} + \psi_\mathrm{s} & E_\mathrm{s} - \psi_\mathrm{s} \\ \psi_\mathrm{w} & -2\psi_\mathrm{w} & \psi_\mathrm{w} \end{bmatrix} \begin{Bmatrix} \mathsf{C}_{1212} \\ \mathsf{C}_{1221} \\ \mathsf{C}_{2121} \end{Bmatrix} = \begin{Bmatrix} S_\mathrm{s} \\ S_\mathrm{s} \\ \mu_3 \end{Bmatrix} \tag{11}$$

The evaluation of in-plane flexural moduli D_{3131} and D_{3232} requires to adopt deformed configurations that cannot be periodic. In the present work the tests have been made on square representative volume elements whose size is $2e = 26$ cm, and the schemes of the two direct tests are shown in Fig. 8, being $K_{31} = K_{32} = \psi_3/e$.

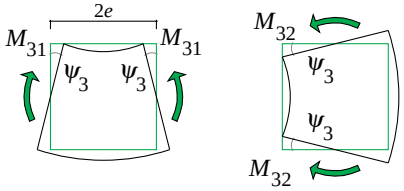

Fig. 8. Scheme of the tests for identification of Cosserat flexural elasticities.

Table 1
Cosserat elastic moduli ($E_b = 10000$ MPa, $E_h/E_v = 10$, $v = 0.1$)

$\mathrm{Log}\frac{E_b}{E_h}$	C_{1111} 10^6 (N/m^2)	C_{1122} 10^6 (N/m^2)	C_{2222} 10^6 (N/m^2)	C_{1212} 10^6 (N/m^2)	C_{1221} 10^6 (N/m^2)	C_{2121} 10^6 (N/m^2)	D_{3131} 10^6 (N)	D_{3232} 10^6 (N)
Rectangular block texture								
1	4858	284.0	4110	1791	684.3	4656	25.66	22.79
2	1248	16.78	609.8	247.8	196.9	642.1	7.113	3.401
3	149.5	0.917	64.11	26.85	22.50	66.94	1.061	0.358
4	15.25	0.082	6.445	2.712	2.283	6.725	0.115	0.036
Square block texture								
1	1873	252.9	5569	2377	856.9	1671	10.17	31.13
2	287.7	23.46	1121	369.9	144.2	285.3	1.511	6.298
3	30.86	1.987	124.9	39.36	15.53	30.84	0.161	0.702
4	3.110	0.194	12.63	3.962	1.565	3.110	0.016	0.071

Table 1 reports the elastic moduli identified for the rectangular and the square block textures in correspondence of different values assigned to the Young moduli of the material components.

3. Rigid element discrete model

Adopting rigid elements (Casolo, 2004), a plane solid body $\Omega \subset \Re^2$ is partitioned into m quadrilaterals ω^i so that no vertex of one quadrilateral element lies on the edge of another element. Given a global Cartesian coordinate frame $\{O, x, y\}$, the deformed configuration of the discrete model is described by the displacements and rotation $\{u_i, v_i, \psi_i\}$ of the local reference frames $\{o^i, \xi^i, \eta^i\}$ fixed to the barycentre of each moving element, as shown in Fig. 9. Thus, the whole kinematic configuration is described by the $3m$ Lagrangian coordinates assembled in the vector $\{u\}$:

$$\{u\}^{\mathrm{T}} = \{u_1, v_1, \psi_1, u_2, v_2, \psi_2, \ldots, u_m, v_m, \psi_m\} \tag{12}$$

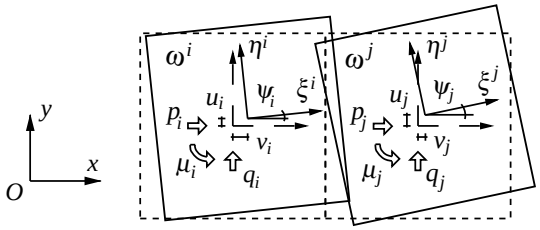

Fig. 9. Displaced couple of rigid elements with evidence of the adopted notation.

The external load is applied considering the undeformed geometry, and the three resultants acting on each element ω^i are assembled into a vector of generalised external load $\{p\}$, conjugated with vector $\{u\}$, as follows:

$$\{p\}^{\mathrm{T}} = \{p_1, q_1, \mu_1, p_2, q_2, \mu_2, \ldots, p_m, q_m, \mu_m\} \tag{13}$$

The elastic devices that connect each couple of elements are placed in correspondence of three connection points named P, Q and R, and are represented like line-springs, as shown in Fig. 10, on the left. Two *normal elastic connections* are placed at the external points P and R, at distance b from Q, while a *shear elastic connection* is placed in the mid-point Q. Axial strains ε^P and ε^R are associated with the volumes of pertinence V^P and V^R, while a shear strain ε^Q is associated with volume $V^Q = V^P + V^R$. The vector of *generalised strain* $\{\varepsilon\}$ and the diagonal matrix of volumes $[V]$ are thus assembled as follows:

$$\{\varepsilon\}^{\mathrm{T}} = \left\{\varepsilon_1^P, \varepsilon_1^Q, \varepsilon_1^R, \varepsilon_2^P, \varepsilon_2^Q, \varepsilon_2^R, \ldots, \varepsilon_r^P, \varepsilon_r^Q, \varepsilon_r^R\right\} \tag{14}$$

$$[V] = \mathrm{Diag}\left\{V_1^P, V_1^Q, V_1^R, V_2^P, V_2^Q, V_2^R, \ldots, V_r^P, V_r^Q, V_r^R\right\} \tag{15}$$

being r the number of sides that connect all the elements of the discrete model. Given the geometry shown in Fig. 10, on the right, and assuming small displacements, the relation between the strain measures and the Lagrangian coordinates for a couple of adjoining elements ω^i and ω^j is

$$\begin{Bmatrix} \varepsilon^P \\ \varepsilon^Q \\ \varepsilon^R \end{Bmatrix} = -\frac{1}{h_i + h_j} \begin{bmatrix} \cos\alpha & \sin\alpha & [\sin(\alpha-\theta_i)d_i + b] \\ -\sin\alpha & \cos\alpha & [\cos(\alpha-\theta_i)d_i] \\ \cos\alpha & \sin\alpha & [\sin(\alpha-\theta_i)d_i - b] \end{bmatrix} \begin{Bmatrix} u_i \\ v_i \\ \psi_i \end{Bmatrix} + \frac{1}{h_i + h_j} \begin{bmatrix} \cos\alpha & \sin\alpha & [\sin(\alpha-\theta_j)d_j + b] \\ -\sin\alpha & \cos\alpha & [\cos(\alpha-\theta_j)d_j] \\ \cos\alpha & \sin\alpha & [\sin(\alpha-\theta_j)d_j - b] \end{bmatrix} \begin{Bmatrix} u_j \\ v_j \\ \psi_j \end{Bmatrix} \tag{16}$$

The linearity of (16), permits to express the strain–displacement relations for the whole model by considering a $3r \times 3m$ matrix $[B]$:

$$\{\varepsilon\} = [B]\{u\} \tag{17}$$

The definition of an external virtual work $\overline{\mathscr{W}}_{\mathrm{e}}$ of the discrete system, and the balance with the corresponding internal virtual work $\overline{\mathscr{W}}_i$ permits to introduce a measure of stress $\{\sigma\}$ conjugated in virtual work to the strain assigned to each connecting device

$$\overline{\mathscr{W}}_{\mathrm{e}} = \{\overline{u}\}^{\mathrm{T}}\{p\} \tag{18}$$

$$\overline{\mathscr{W}}_i = \{\overline{\varepsilon}\}^{\mathrm{T}}[V]\{\sigma\} \tag{19}$$

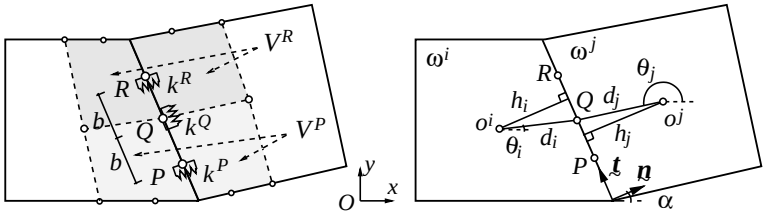

Fig. 10. Couple of rigid elements ω^i and ω^j of irregular shape with evidence of the tributary volumes V^R and V^P and the elastic devices.

being $\{\sigma\}$ the vector of *generalised stress* assembled as follows:

$$\{\sigma\}^{\mathrm{T}} = \left\{\sigma_1^P, \sigma_1^Q, \sigma_1^R, \sigma_2^P, \sigma_2^Q, \sigma_2^R, \ldots, \sigma_r^P, \sigma_r^Q, \sigma_r^R\right\} \tag{20}$$

Obeying the spirit of Hooke's law, a linear constitutive relation is assumed

$$\{\sigma\} = [D]\{\varepsilon\} \tag{21}$$

where $[D]$ is the *constitutive matrix* of the connecting devices

$$[D] = \mathrm{Diag}\left\{k_1^P, k_1^Q, k_1^R, k_2^P, k_2^Q, k_2^R, \ldots, k_r^P, k_r^Q, k_r^R\right\} \tag{22}$$

At this point the balance of virtual work gives

$$\{\overline{u}\}^{\mathrm{T}}\{p\} = \overline{\mathscr{W}}_{\mathrm{e}} = \overline{\mathscr{W}}_i = \{\overline{u}\}^{\mathrm{T}}[B]^{\mathrm{T}}[V][D][B]\{u\} \tag{23}$$

and the arbitrary of $\{\overline{u}\}$ leads to the following resolving system:

$$\{p\} = [B]^{\mathrm{T}}[V][D][B]\{u\} = [K]\{u\} \tag{24}$$

being $[K]$ the global generalised stiffness matrix of the discrete system. The size effects and the internal length are taken into account by means of the procedure described in (Casolo, 2004).

4. Relationship between elasticities

This section expounds the relationship between the mechanical characteristics of the connecting devices of rigid elements and a given orthotropic Cosserat material. In the present rigid element formulation, the discrete material model is composed by an assembly of *unit cells* that can be represented as shown in Fig. 11, by the shaded area. These unit cells can be imaged as a sort of "heuristic molecules", in which the rigid elements are "atoms" bonded together by the elastic springs. Given the disposition of the springs,[1] the constitutive behaviour of this material model is governed by six parameters: k_x^A, k_y^A, for the axial stiffnesses along the horizontal and vertical directions; k_{h}^Q, k_{v}^Q, for the shear stiffnesses along the horizontal and vertical directions; b_x, b_y for the distances of the horizontal and vertical axial connections. The reduction from eight to six parameters in the passage from orthotropic Cosserat continuum to rigid elements implies the loss of information about the axial and shear coupling effects due to Poisson coefficient and the Cosserat shear moduli. As a consequence, in the procedure of identification we need to specify with clarity the character of the boundary conditions that involve the displacements or the tractions.

4.1. Axial moduli

The case of simple normal loading acting along two opposite sides parallel to the principal direction of the material is considered with the imposition of traction-free boundary conditions on the other two sides. The following constitutive relations hold:

$$E_{11} = \mathsf{A}_{1111}S_{11}, \quad E_{22} = \mathsf{A}_{2222}S_{22} \tag{25}$$

Using rigid elements, after assigning $\varepsilon_x = E_{11}$, $\varepsilon_y = E_{22}$, $\sigma_x = S_{11}$ and $\sigma_y = S_{22}$, the corresponding situation is described by

$$\varepsilon_x = \frac{\sigma_x}{k_x^A}, \quad \varepsilon_y = \frac{\sigma_y}{k_y^A} \tag{26}$$

[1] The disposition of the springs in the present formulation implies to neglect the axial coupling due to Poisson effect, nevertheless this approximation is not necessarily intrinsic of the model.

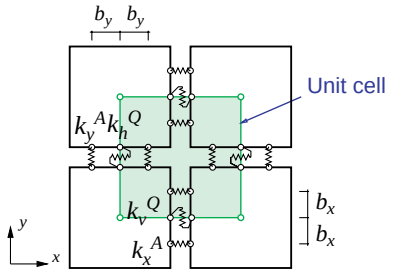

Fig. 11. Heuristic representation of a unit cell made of rigid elements.

and thus we have[2]

$$k_x^A = \frac{1}{\mathsf{A}_{1111}} = \frac{\mathsf{C}_{1111}\mathsf{C}_{2222} - \mathsf{C}_{1122}^2}{\mathsf{C}_{2222}}$$
$$k_y^A = \frac{1}{\mathsf{A}_{2222}} = \frac{\mathsf{C}_{1111}\mathsf{C}_{2222} - \mathsf{C}_{1122}^2}{\mathsf{C}_{1111}} \tag{27}$$

4.2. Shear moduli

In the case of symmetric shear loading ($S_{12} = S_{21} = S_s$) and absence of macro-rotation ($E_w = 0$), the constitutive relation of the orthotropic Cosserat continuum gives:

$$\begin{bmatrix} \mathsf{A}_{1212} & \mathsf{A}_{1221} \\ \mathsf{A}_{1221} & \mathsf{A}_{2121} \end{bmatrix} \begin{Bmatrix} S_s \\ S_s \end{Bmatrix} = \begin{Bmatrix} E_{12} \\ E_{21} \end{Bmatrix} = \begin{Bmatrix} E_s + \psi_3 \\ E_s - \psi_3 \end{Bmatrix} \tag{28}$$

The situation with rigid elements is shown in Fig. 12, where we note that distinct shear deformations are associated to the vertical and horizontal shear springs. After defining the *mean shear strain* as $\varepsilon_s = u/e = v/e$ and the *local rigid rotation ratio* as $\rho = \psi/\varepsilon_s$, the generalised shear strains for the vertical and the horizontal connecting devices are

$$\varepsilon_h = \varepsilon_s + \psi = \varepsilon_s(1 + \rho)$$
$$\varepsilon_v = \varepsilon_s - \psi = \varepsilon_s(1 - \rho) \tag{29}$$

As a consequence, the corresponding constitutive relation is

$$\begin{bmatrix} 1/k_h^Q & 0 \\ 0 & 1/k_v^Q \end{bmatrix} \begin{Bmatrix} \sigma_s \\ \sigma_s \end{Bmatrix} = \begin{Bmatrix} \varepsilon_h \\ \varepsilon_v \end{Bmatrix} = \begin{Bmatrix} \varepsilon_s + \psi \\ \varepsilon_s - \psi \end{Bmatrix} \tag{30}$$

[2] In the case of plane stress orthotropic Cauchy continuum, the constitutive relation is often written adopting the "engineering constants" as follows (Lekhnitskii, 1968)

$$\begin{Bmatrix} \varepsilon_{xx} \\ \varepsilon_{yy} \\ \varepsilon_{xy} \end{Bmatrix} = \begin{bmatrix} \frac{1}{E_x} & -\frac{\nu_{yx}}{E_y} & 0 \\ -\frac{\nu_{xy}}{E_x} & \frac{1}{E_y} & 0 \\ 0 & 0 & \frac{1}{2G} \end{bmatrix} \begin{Bmatrix} \sigma_{xx} \\ \sigma_{yy} \\ \sigma_{xy} \end{Bmatrix}$$

being $\nu_{xy}E_y = \nu_{yx}E_x$. As a consequence, in this case we obtain $k_x^A = E_x$ and $k_y^A = E_y$ from Eq. (27).

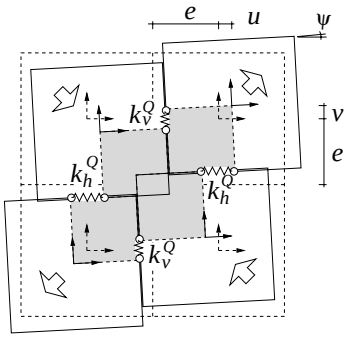

Fig. 12. Assemblage of four rigid elements subjected to shear loading.

Thus, after assigning $\varepsilon_h = E_{12}$, $\varepsilon_v = E_{21}$ and $\sigma_s = S_s$, the comparison of Eqs. (28) and (30) leads to[3,4]

$$k_h^Q = \frac{1}{A_{1212} + A_{1221}} = \frac{C_{1212}C_{2121} - C_{1221}^2}{C_{2121} - C_{1221}}$$
$$k_v^Q = \frac{1}{A_{1221} + A_{2121}} = \frac{C_{1212}C_{2121} - C_{1221}^2}{C_{1212} - C_{1221}} \tag{31}$$

Parameter ρ is related to the orthotropic shear moduli of the Cosserat continuum by

$$\frac{k_h^Q}{k_v^Q} = \frac{\varepsilon_v}{\varepsilon_h} = \frac{1-\rho}{1+\rho} = \frac{C_{1212} - C_{1221}}{C_{2121} - C_{1221}} \tag{32}$$

and thus

$$\rho = \frac{C_{2121} - C_{1212}}{C_{2121} + C_{1212} - 2C_{1221}} \tag{33}$$

[3] The engineering shear modulus G can be obtained as the ratio between the mean shear stress S_s and the mean shear strain E_s as follows:

$$G = \frac{S_s}{2E_s} = \frac{C_{1212}C_{2121} - C_{1221}^2}{C_{2121} + C_{1212} - 2C_{1221}}$$

on the other hand, if we consider an isotropic Cosserat material for which $C_{1212} = C_{2121} = G$, then the limit of Eq. (31) toward a Cauchy continuum gives

$$\lim_{C_{1221} \to G} k_h^Q = \lim_{C_{1221} \to G} k_v^Q = 2G$$

[4] It is worth considering also the case in which the elastic tensor C is diagonal, as proposed in Masiani et al. (1995); Sulem and Mühlhaus (1997); Trovalusci and Masiani (1999), that considered composites made by rigid blocks arranged with a masonry-like texture. In this case $C_{1221} = 0$, and the following simple relations hold:

$$k_h^Q = C_{1212}$$
$$k_v^Q = C_{2121}$$

while a "symmetric" shear stiffness can be defined as

$$k^S = \frac{\sigma_s}{\varepsilon_s} = \frac{k_h}{1-\rho} = \frac{k_v}{1+\rho} = \frac{(C_{1212}C_{2121} - C_{1221}^2)(C_{2121} + C_{1212} - 2C_{1221})}{2(C_{2121} - C_{1212})(C_{1212} - C_{1221})} \tag{34}$$

4.3. Flexural moduli and characteristic length

The case of in-plane flexural bending is shown in Fig. 13. The curvatures of the continuum and the strains in the connecting devices of rigid elements are related to the angle of rotation ψ according to

$$\begin{aligned} &K_{31} = K_{32} = \psi/e \\ &\varepsilon_x = \psi\frac{b_x}{e}, \quad \varepsilon_y = \psi\frac{b_y}{e} \end{aligned} \tag{35}$$

while the couple stresses of the continuum are related to the generalised stresses in the connection devices by

$$M_{31} = \sigma_x b_x = k_x^A \varepsilon_x b_x, \quad M_{32} = \sigma_y b_y = k_y^A \varepsilon_y b_y \tag{36}$$

From Eqs. (35) and (36), after introducing the constitutive relations, the distances b_x and b_y are obtained as a function of in-plane flexural stiffness as follows:

$$\begin{aligned} b_x &= \beta_x e = \sqrt{\frac{D_{3131}}{k_x^A}} \\ b_y &= \beta_y e = \sqrt{\frac{D_{3232}}{k_y^A}} \end{aligned} \tag{37}$$

The outlined procedure gives the values reported in Table 2 that is related to Table 1. It is worth observing that the local rotation of rigid elements is in accord with the symmetric shear strain ($\rho = \psi/\varepsilon_s > 0$) for the rectangular block texture, while the opposite happens when approximating the square block texture. Moreover, modelling the in-plane flexural stiffness for high E_b/E_h ratios requires a significant increase of β_x in the case of rectangular block texture, while this does not happen for the square block texture. These facts display the different relevance of the micro-structure effects for the two texture. Finally, it must be mentioned that present values are coherent and identical to those obtained by the direct identification procedure outlined in (Casolo, 2004).

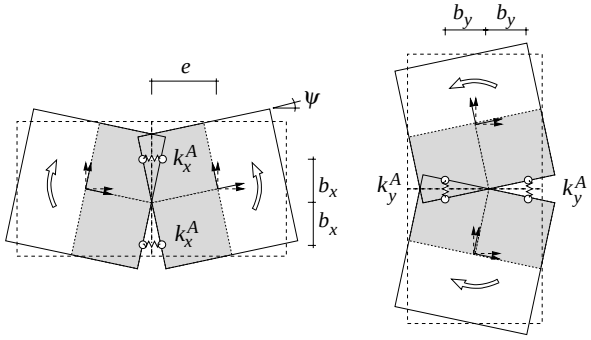

Fig. 13. Couple of rigid elements subjected to in-plane bending.

Table 2
Rigid element parameters ($E_b = 10000$ MPa, $E_h/E_v = 10$, $v = 0.1$)

$\text{Log}\frac{E_b}{E_h}$	k_x 10^6 (N/m^2)	k_y 10^6 (N/m^2)	k^S 10^6 (N/m^2)	ρ	β_x	β_y
Rectangular block texture						
1	4838	4093	4547	0.564	0.560	0.574
2	1247	609.6	1318	0.795	0.581	0.575
3	149.5	64.10	162.9	0.822	0.648	0.575
4	15.25	6.444	16.66	0.824	0.669	0.575
Square block texture						
1	1862	5535	3054	−0.303	0.568	0.577
2	287.2	1119	488.1	−0.231	0.558	0.577
3	30.83	124.8	52.18	−0.217	0.556	0.577
4	3.107	12.62	5.254	−0.216	0.556	0.577

5. Numerical results and comparisons

A number of numerical tests have been made with the aim of comparing the performance of three macroscopic approaches: two finite element models based on Cauchy and Cosserat continuum theory, and the proposed rigid element model. In general, the mean response of the three macroscopic approaches in terms of global displacements proved similar and adequate in the linear elastic field. The main difference is expected in the description of the strain and stress maps, due to the non-symmetry of the Cosserat strain and stress tensors, and the different characteristics of the shear connecting devices of the proposed rigid elements.

The case of the composite masonry-like wall shown in Fig. 14 is presented in detail with the aim to evaluate the influence of the texture on the mechanism of diffusion of a load applied on a limited area, and in particular to compare the capability of different macroscopic approaches to retain memory of the original composite behaviour.

Two refined finite element meshes of the rectangular and square block composite textures have been considered as reference, adopting the computer code *Abaqus* (Hibbitt et al., 2004). Plane stress 4-node bilinear continuum solid elements have been used, with a total number of 41302 and 39734 degrees of freedom respectively. These two composite models are made of Cauchy isotropic materials with fixed Poisson coefficient $v = 0.1$ and Young modulus $E_b = 10000$ MPa for the blocks. Different values, in the range 1−10000, have been assumed for the ratio of Young moduli of the blocks and of the horizontal joints E_b/E_h, while Young modulus of the vertical joint material E_v is always $E_v = E_h/10$. Very high E_b/E_h values are considered with the purpose of studying situations in which the joints' material is highly degraded.

Regular meshes of 28×28 elements are adopted for the macroscopic models presented here. Plane stress 4-node bilinear finite elements are used for both the Cauchy and Cosserat homogeneous continuum

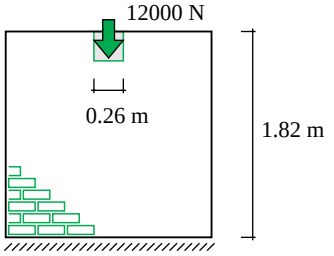

Fig. 14. Scheme of the square wall loaded by a vertical load distributed in the shaded square area; the thickness is 0.12 m.

material models, with a total number of 1624 and 2436 degrees of freedom respectively. In particular, Cosserat linear elasticity has been implemented by assigning to each node the three degrees of freedom u_1, u_2, ψ_3, while the displacements and the local rotation are interpolated by bilinear shape functions. Then, the strains are evaluated by Eq. (4) and the constitutive relation is given by Eq. (8). The assembly and the resolution of the governing equations follows the same scheme of a classic finite element code based on a displacement approach (Zani, 2004). Finally, the rigid element model, with 2352 degrees of freedom, has been calculated by means of the same code already implemented in (Casolo, 2004).

The response of the different models in terms of global displacement is quite similar, as shown qualitatively in Fig. 15, and also the values of maximum vertical displacement reported in Table 3 manifest a good accord if we consider the great difference of the alternative approaches. All the models are able to distinguish the response of the two textures in terms of global displacements, and in particular the different width

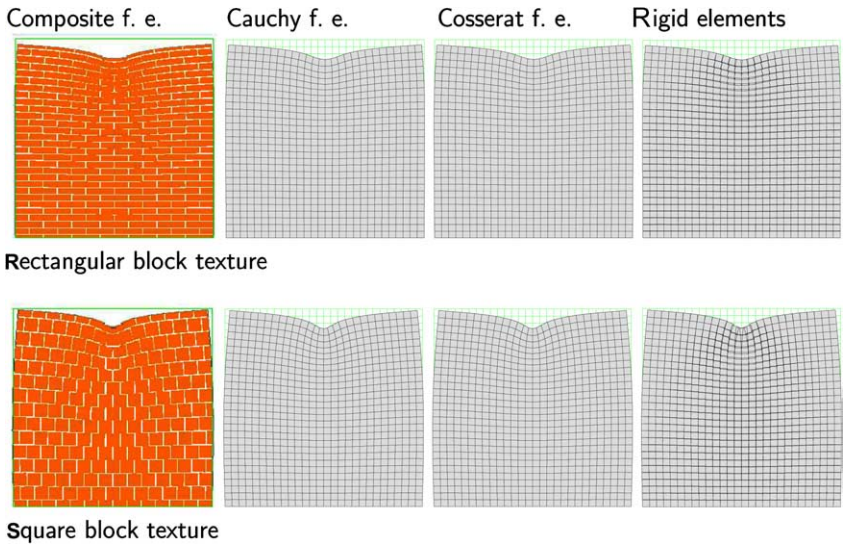

Fig. 15. Deformation maps. Comparison of the refined composite finite element models, on the left, with the three macroscopic approaches; case of $\mathrm{Log}\frac{E_\mathrm{b}}{E_\mathrm{h}} = 2$.

Table 3
Maximum vertical displacement [m]; $E_\mathrm{b} = 10000$ MPa, $E_\mathrm{h}/E_\mathrm{v} = 10$, $v = 0.1$

$\mathrm{Log}\frac{E_\mathrm{b}}{E_\mathrm{h}}$	Composite finite elements	Cauchy finite elements	Cosserat finite elements	Specific rigid elements
dof	41302/39734	1624	2436	2352
Rectangular block texture				
1	4.392×10^{-5}	4.389×10^{-5}	4.339×10^{-5}	4.336×10^{-5}
2	2.741×10^{-4}	2.827×10^{-4}	2.803×10^{-4}	2.763×10^{-4}
3	2.473×10^{-3}	2.650×10^{-3}	2.630×10^{-3}	2.573×10^{-3}
4	2.414×10^{-2}	2.631×10^{-2}	2.611×10^{-2}	2.550×10^{-2}
Square block texture				
1	4.027×10^{-5}	3.844×10^{-5}	3.834×10^{-5}	3.831×10^{-5}
2	2.136×10^{-4}	2.024×10^{-4}	2.019×10^{-4}	2.007×10^{-4}
3	1.937×10^{-3}	1.836×10^{-3}	1.831×10^{-3}	1.817×10^{-3}
4	1.917×10^{-2}	1.817×10^{-2}	1.812×10^{-2}	1.799×10^{-2}

and shape of the valley induced by the load on the top side of the wall. This fact indicates that in this case an orthotropic Cauchy material seems adequate in order to obtain a good approximation of the global displacements and deformed shape.

A better understanding of the texture effects requires to examine the maps of strain and stress. The maps shown in Figs. 16 and 17, relative to the finite element meshes of the composite walls, clearly reveal the trace of texture geometry, with the strains that primarily involve the weak material of the joints while the stresses find their way toward the base preferably passing through the blocks. It is worth to observe two aspects that are consequence of the different texture geometry: (i) the angle of diffusion of the load, and in particular of

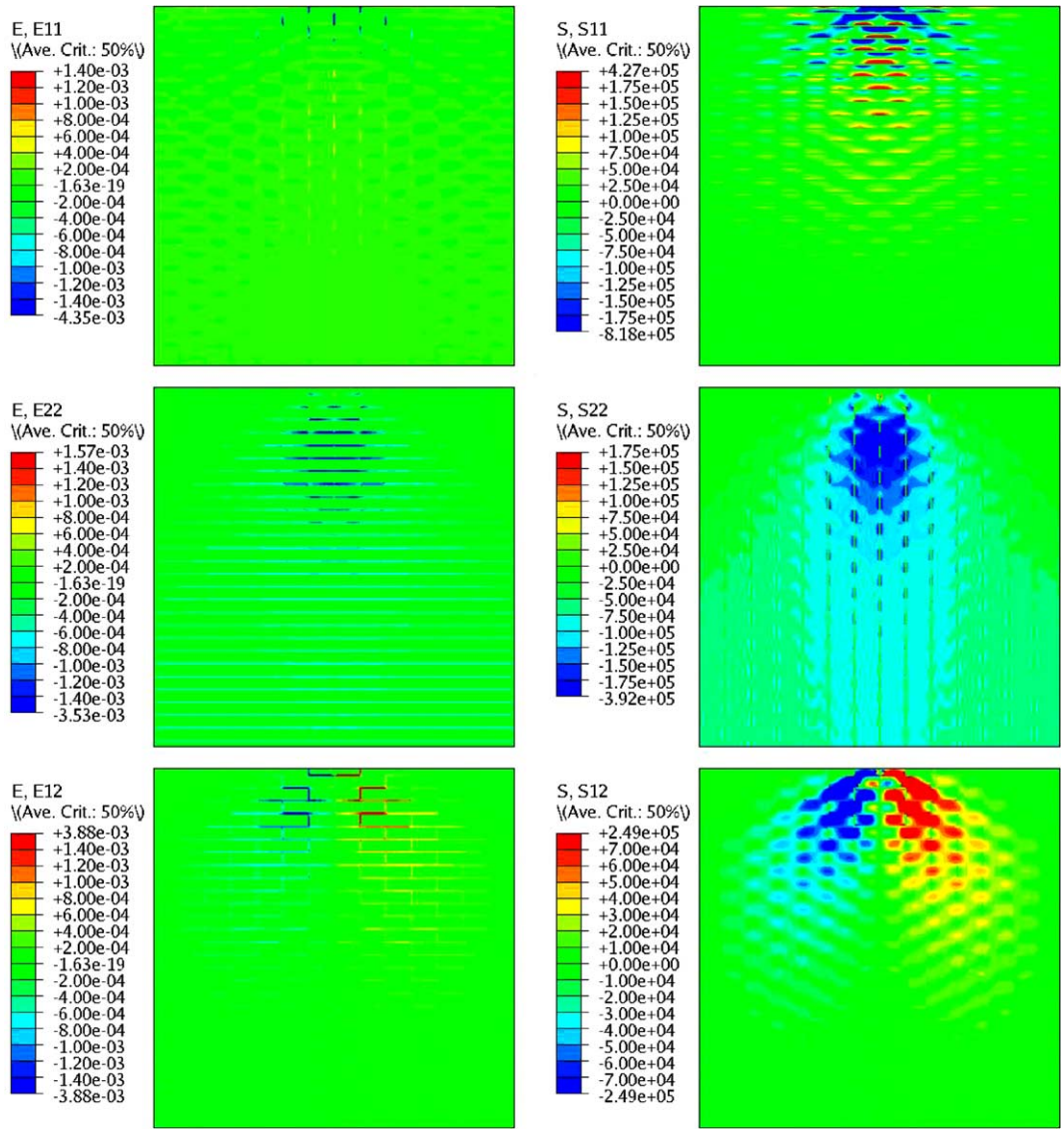

Fig. 16. Refined finite element model of the wall made with the rectangular block texture. Strain and stress maps. Case with $\mathrm{Log}\frac{E_b}{E_h} = 2$.

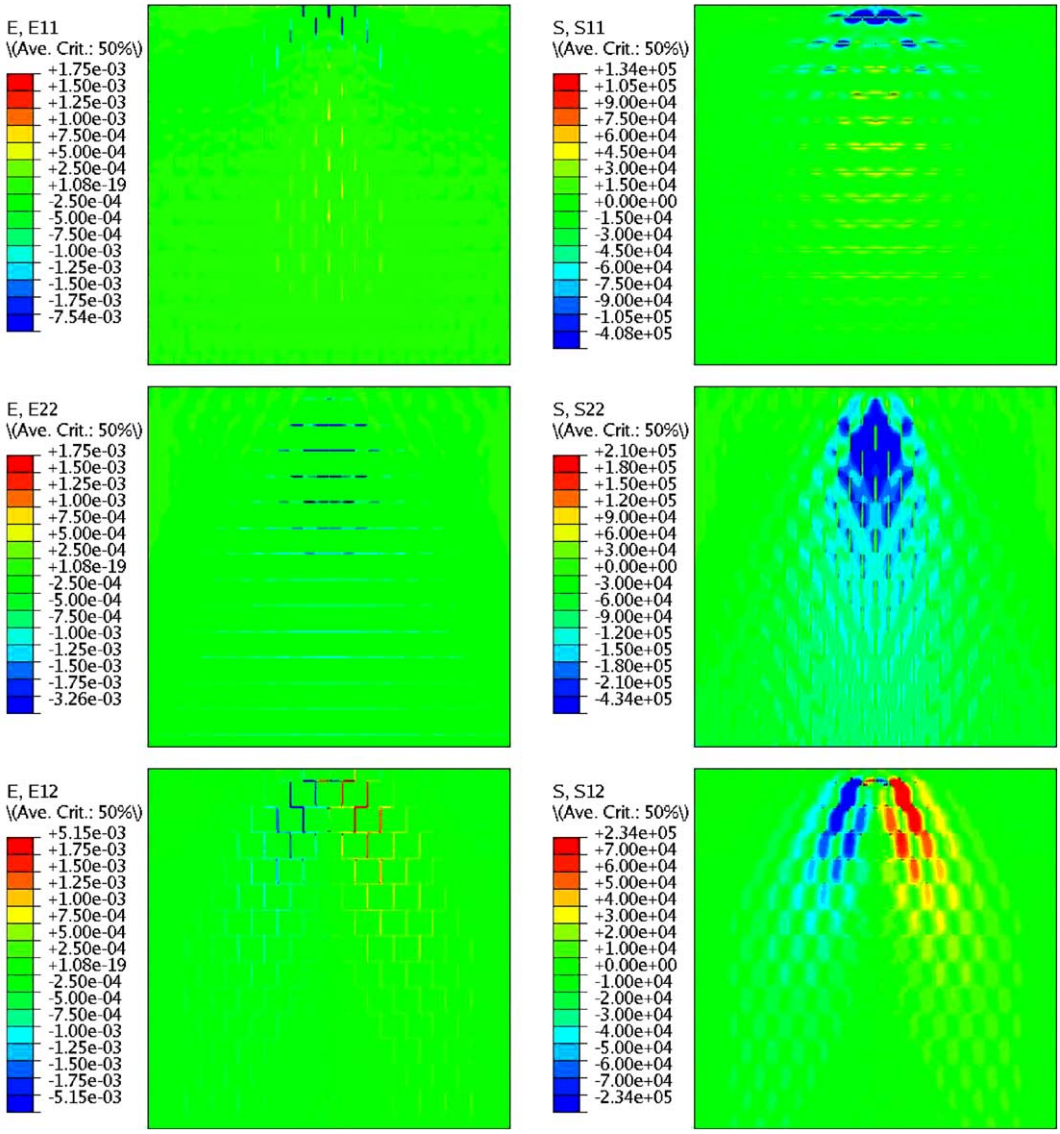

Fig. 17. Refined finite element model of the wall made with the square block texture. Strain and stress maps. Case with $\mathrm{Log}\frac{E_b}{E_h} = 2$.

the shear stress S_{12} is governed by the geometry and arrangement of the blocks, (ii) the deformation mechanism, and in particular the shear strain of the rectangular block texture tends to involve in preference the material of the horizontal joints, while for the square block texture the deformation involve mainly the vertical joints. The first observation reveals the need of adopting an orthotropic material model to describe the stress distribution at the macro-scale. The second observation displays the loss of information related with the choice of a macroscopic description that adopts a symmetric strain tensor, $E_s = E_{12} = E_{21}$, and suggests the adoption of a more sophisticated material model to overcome this limitation.

The three macro-scale solutions are compared in terms of strain/stress components by the colour maps shown in Figs. 18–21. Considering finite element solutions, the axial components are plotted as constant on

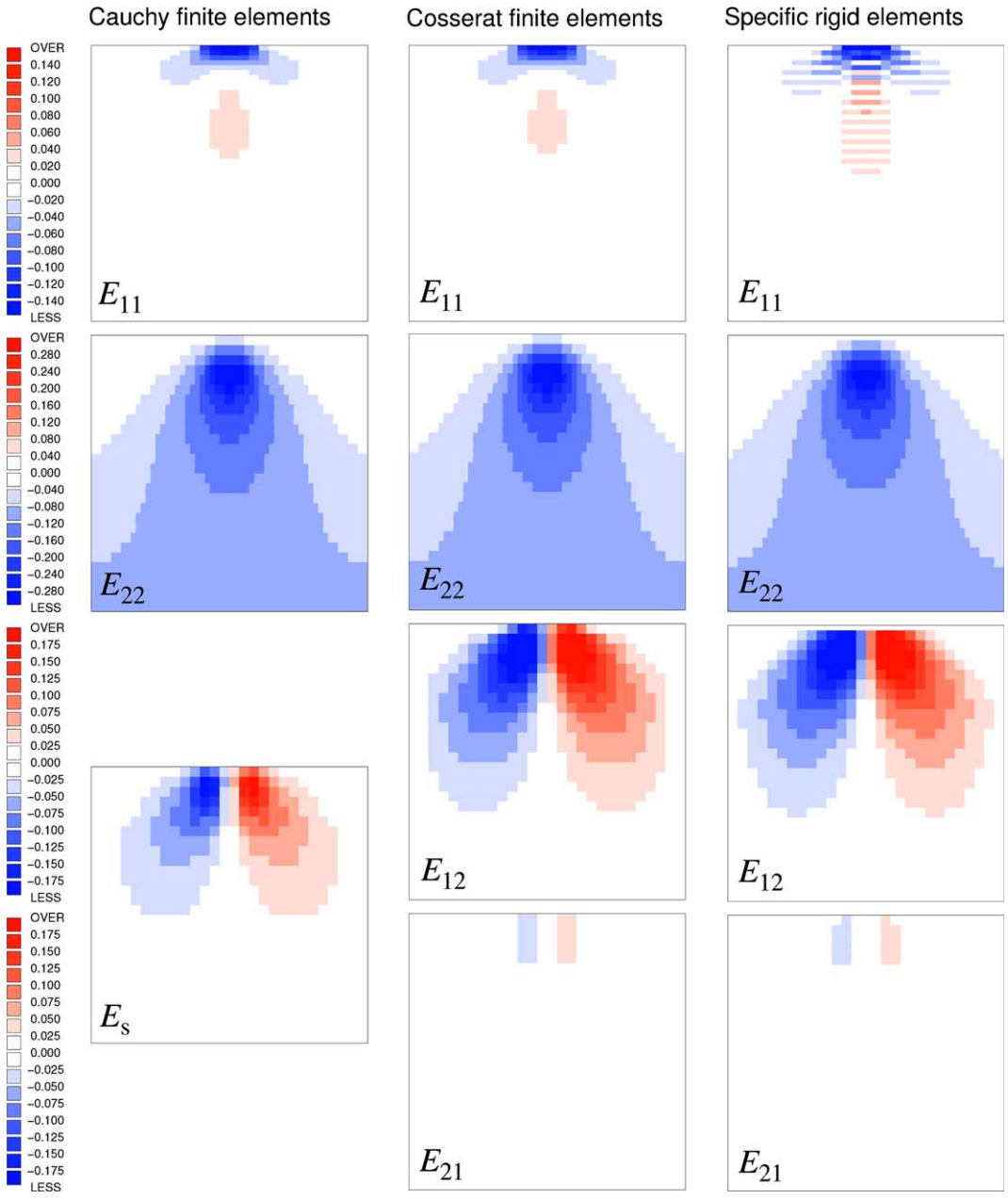

Fig. 18. Comparison of the macro-scale maps of strain (×1000) for the case of rectangular block texture. Case with $\mathrm{Log}\frac{E_b}{E_h} = 2$.

each quarter of element by assigning the value at the corresponding Gauss point, while the shear components are plotted as constant on the entire element by assigning the average value of the four Gauss points. This smoothing has been assumed since shear values suffer for a slight fluctuation into each element due to the contribute of the local-rotation ψ_3. In the case of the specific rigid elements, the colour maps are simply based on the values of the generalised strain and stress of the springs as defined by Eqs. (16), (21), and these

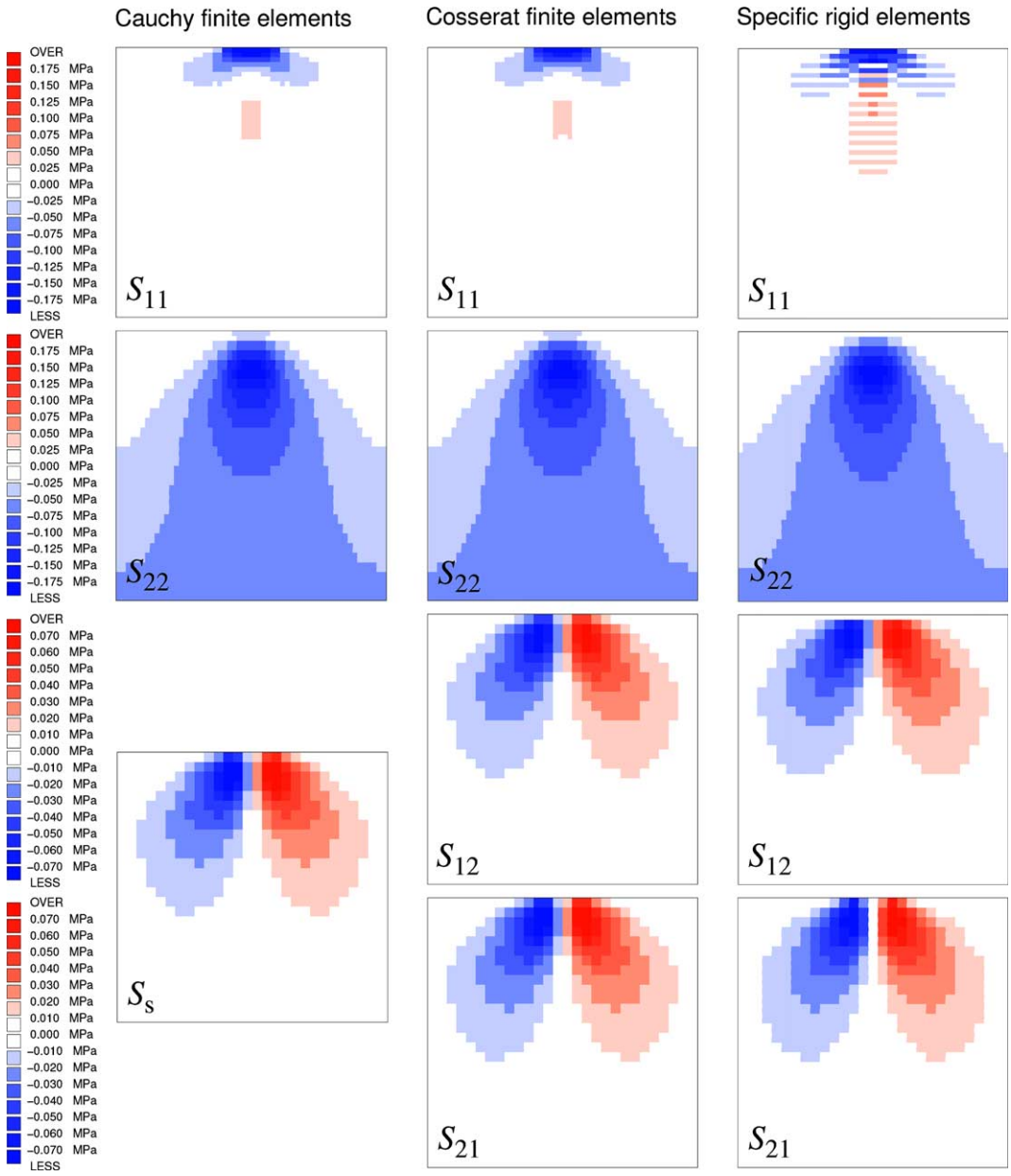

Fig. 19. Comparison of the macro-scale maps of stress for the case of rectangular block texture. Case with $\mathrm{Log}\frac{E_b}{E_h} = 2$.

values are plotted as constant for each quarter of element without smoothing. The stress maps shown in Figs. 19 and 21 display small differences between the three macroscopic models for both masonry-like textures. In particular, the three models give an adequate estimate of the values of the stress components that pass through the blocks of the heterogeneous composite materials, and also the shape of the areas of diffusion of the load are comparable with the maps reported in Figs. 16 and 17. The situation is quite different for what regards the strain maps shown in Figs. 18 and 20. In this case, the Cosserat continuum and the

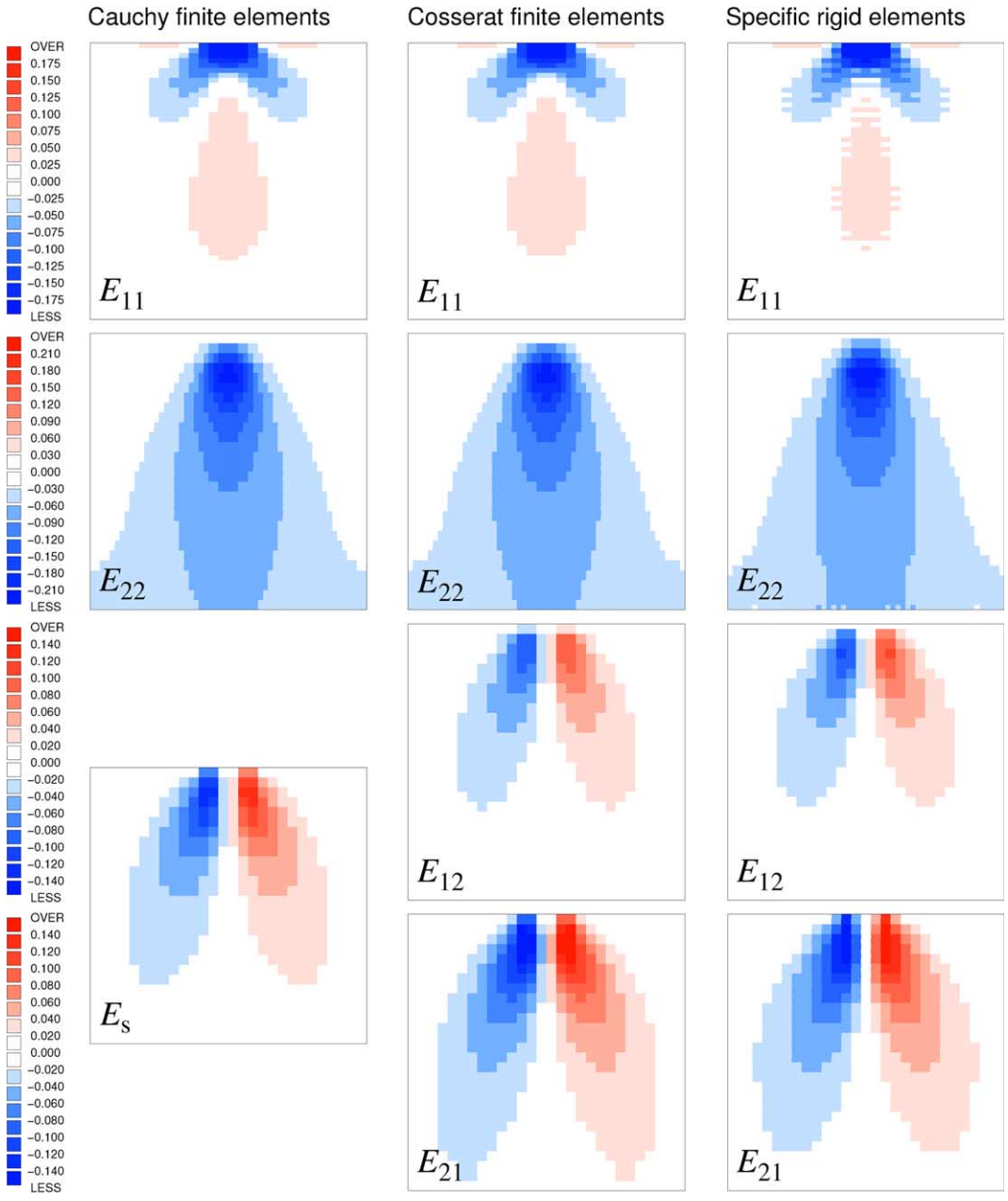

Fig. 20. Comparison of the macro-scale maps of strain (×1000) for the case of square block texture. Case with $\mathrm{Log}\frac{E_h}{E_h} = 2$.

proposed rigid element model clearly distinguish the strain components E_{12} and E_{21}, with a prevalence of E_{12} for the macro-scale maps relatives to the rectangular block texture, while E_{21} prevails for the square block texture. Recalling the geometric meaning of Eqs. (5) and (29), we note that E_{12} can be related with the shear deformation of the horizontal joints of the composite texture, while E_{21} can be related with the shear deformation of the vertical joints, and thus there is a substantial accord with the previous observation

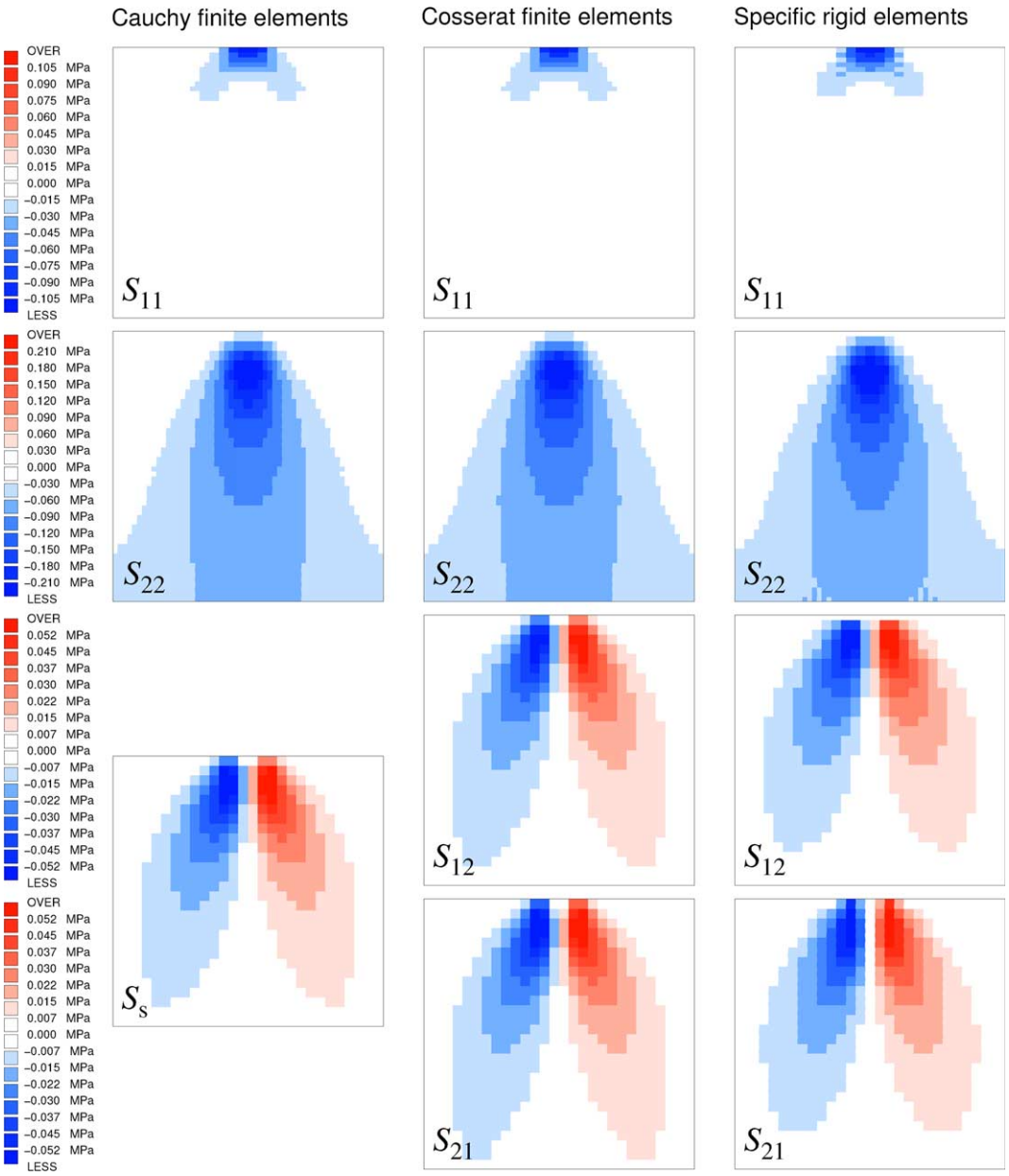

Fig. 21. Comparison of the macro-scale maps of stress for the case of square block texture. Case with $\mathrm{Log}\frac{E_b}{E_h} = 2$.

on the strain maps of Figs. 16 and 17. In describing deformation, Cosserat finite elements and the proposed rigid element model clearly demonstrate their superiority respect to Cauchy finite elements. This feature can be important in the formulation of a macro-scale constitutive model with the capability of describing the progressive degradation of a structured material, and it can also be useful in modelling Mohr-Coulomb effects that are different depending on the direction of the joints.

6. Final remarks

The present contribution expounds the relation between orthotropic Cosserat continuum and a specific rigid element approach, with the objective to model plane regular structured materials at the macro-scale. Given two masonry-like composite textures, the corresponding orthotropic Cosserat elastic tensor is obtained by means of a computational homogenisation procedure, then the characteristics of rigid elements are derived and related to those of the continuum material. This passage implies a lose of information due to the contraction of the number elastic parameters from eight to six, nevertheless the numerical results show a substantial equivalence of performance between these two approaches. In particular they are able to retain memory of the different shear deformation mechanism of the original textures with reduced computational effort.

The adoption of a mechanistic discrete model that concentrates elasticity into simple connecting springs can give some advantage in term of simplicity respect to a continuum model, in particular when there is the need of implementing a constitutive relation that requires the description of cyclic responses and degradation (Casolo, 2000). A mechanistic approach can be useful also in the macroscopic formulation of solid mechanics problems when dealing with composite materials that change their micro-structure characteristics when loading in the non-linear field (Casolo, 2004). In this perspective, as an engineering alternative to the continuum approach, it is possible to imagine a sort of ''heuristic-molecular'' material model in which the disposition and the characteristics of the spring devices connecting the elements of a given unit-cell describe at the macro-scale the essential micro-structure aspects of an heterogeneous structured material.

Acknowledgement

The author wish to express his gratitude to Dr. Nicola Zani, Dipartimento di Costruzioni, University of Florence, for the calculations made using his original Cosserat finite element code, *ORZATA* (Zani, 2004).

References

Anthoine, A., 1995. Derivation of the in-plane elastic characteristics of masonry through homogenization theory. International Journal of Solids and Structures 32 (2), 137–163.

Bouyge, F., Jasiuk, I., Ostoja-Starzewski, M., 2001. A micromechanically based couple-stress model of an elastic two-phase composite. International Journal of Solids and Structures 38 (10–13), 1721–1735.

Casolo, S., 2000. Modelling the out-of-plane seismic behaviour of masonry walls by rigid elements. Earthquake Engineering and Structural Dynamics 29 (12), 1797–1813.

Casolo, S., 2004. Modelling in-plane micro-structure of masonry walls by rigid elements. International Journal of Solids and Structures 41 (13), 3625–3641.

Forest, S., Sab, K., 1998. Cosserat overall modeling of heterogeneous materials. Mechanics Research Communication 25 (4), 449–454.

Forest, S., Pradel, F., Sab, K., 2001. Asymptotic analysis of heterogeneous Cosserat media. International Journal of Solids and Structures 38 (26–27), 4585–4608.

Griffiths, D.V., Mustoe, G.G.W., 2001. Modelling of elastic continua using a grillage of structural elements based on discrete element concepts. International Journal for Numerical Methods in Engineering 50 (7), 1759–1775.

Hibbitt, Karlsson, Sorensen, Inc., 2004. *ABAQUS* Manuals, version 6.4.

Kawai, T., 1978. New discrete models and their application to seismic response analysis of structures. Nuclear Engineering and Design 48, 207–229.

Lekhnitskii, S.G., 1968. Anisotropic Plates. Gordon and Breach Science Publishers.

Masiani, R., Rizzi, N., Trovalusci, P., 1995. Masonry as structured continuum. Meccanica 30 (6), 673–683.

Mühlhaus, H.-B., 1993. Continuum models for layered and blocky rock. In: Fairhurst, C. (Ed.), Comprehensive Rock Engineering, Vol. II. Pergamon Press, pp. 209–230.

Nakamura, S., Benedict, R., Lakes, R., 1984. Finite element method for orthotropic micropolar elasticity. International Journal of Engineering Science 22 (3), 319–330.

Providas, E., Kattis, M.A., 2002. Finite element method for in plane Cosserat elasticity. Computers & Structures 80, 2059–2069.

Ristinmaa, M., Vecchi, M., 1996. Use of couple-stress theory in elasto-plasticity. Computer Methods in Applied Mechanics and Engineering 136, 205–224.

Shu, J.Y., King, W.E., Fleck, N.S., 1999. Finite elements for materials with strain gradient effects. International Journal for Numerical Methods in Engineering 44 (3), 373–391.

Sulem, J., Mühlhaus, H.-B., 1997. A continuum model for periodic two-dimensional block structures. Mechanics of Cohesive-Frictional Materials 2, 31–46.

Tonti, E., 2001. A direct discrete formulation of field laws: the cell method. Computer Modeling in Engineering Sciences 2 (2), 237–258.

Trovalusci, P., Masiani, R., 1999. Material symmetries of micropolar continua equivalent to lattices. International Journal of Solids and Structures 36 (14), 2091–2108.

Trovalusci, P., Masiani, R., 2003. Non-linear micropolar and classical continua for anisotropic discontinuous materials. International Journal of Solids and Structures 40 (5), 1281–1297.

van der Sluis, O., Vosbeek, P.H.J., Schreurs, P.J.G., Meijer, H.E.H., 1999. Homogenization of heterogeneous polymers. International Journal of Solids and Structures 36 (21), 3193–3214.

Zani, N., 2004. Technical report. *ORZATA* orthotropic 2-D Cosserat finite element code. Dipartimento di Costruzioni of University of Florence, Italy.